The Astrophysical Journal, 726:22 (8pp), 2011 January 1 doi:10.1088/0004-637X/726/1/22

SEARCHING FOR NEEDLES IN HAYSTACKS—LOOKING FOR GAMMA-RAY BURST γ-RAYS WITH THE *FERMI*/LAT DETECTOR

C. W. Akerlof[1], W. Zheng[1], S. B. Pandey[1,2], and T. A. McKay[1]
[1] Randall Laboratory of Physics, University of Michigan, 450 Church Street, Ann Arbor, MI 48109-1040, USA; cakerlof@umich.edu
[2] Aryabhatta Research Institute of Observational Sciences, Manora Peak, Nainital 263129, India
Received 2010 July 6; accepted 2010 October 23; published 2010 December 10

ABSTRACT

Since the launch of the *Fermi Gamma-ray Space Telescope* on 2008 June 11, 55 gamma-ray bursts (GRBs) have been observed at coordinates that fall within 66° of the *Fermi* Large Area Telescope (LAT) boresight with precise localizations provided by the NASA *Swift* mission or other satellites. Imposing selection cuts to exclude low Galactic latitudes and high zenith angles reduces the sample size to 41. Using matched filter techniques, the *Fermi*/LAT photon data for these fields have been examined for evidence of bursts that have so far evaded detection at energies above 100 MeV. Following comparisons with similar random background fields, two events, GRB 080905A and GRB 091208B, stand out as excellent candidates for such an identification. After excluding the six bright bursts previously reported by the LAT team, the remaining 35 events exhibit an excess of LAT "diffuse" photons with a statistical significance greater than 2σ, independent of the matched filter analysis. After accounting for the total number of photons in the well-localized fields and including estimates of detection efficiency, one concludes that somewhere in the range of 11%–19% of all GRBs within the LAT field of view illuminate the detector with two or more energetic photons. These are the most stringent estimates of the high-energy photon content of GRBs to date. The two new events associated with high-energy photon emission have similar ratios of high- to low-energy fluences as observed previously. This separates them from bursts with similar low-energy fluences by a factor of 10, suggesting a distinct class of events rather than a smooth continuum.

Key words: gamma-ray burst: general

1. INTRODUCTION

One of the more surprising results of the *Compton Gamma-Ray Observatory* was the EGRET discovery of an 18 GeV photon associated with GRB 940217 (Hurley et al. 1994). This was not an entirely unique event; about a half-dozen bursts were seen over the course of the mission with photons above 100 MeV (Catelli et al. 1998; Dingus 2003). Since the GRB spectral energy distribution at lower energies has been well characterized by a modified power law with peak fluxes at energies of the order of 200 keV, the existence of photons at energies 10^4 times higher puts a significant constraint on any viable model of the GRB phenomenon (e.g., Band et al. 2009). The obvious question is whether high-energy photons are associated with all GRBs or only with a small sub-class. We are now in a unique period when two space missions are providing GRB coordinates with arcsecond accuracy (*Swift*; Gehrels et al. 2004) and the ability to measure photon energies to 300 GeV (*Fermi*/LAT; Atwood et al. 2009). Once these two missions cease functioning, the resources to investigate GRBs over a broad energy range are not likely to be available for decades. Thus, it is a matter of some urgency to extract the maximum amount of information from the assets now at hand. Prior to the launch of the *Fermi Gamma-ray Space Telescope*, it was possible to speculate that the LAT instrument would detect more than 200 GRB events per year (Dingus 2003). In the two-year period since the launch of the *Fermi Gamma-ray Space Telescope*, the Gamma-ray Burst Monitor (GBM; Meegan et al. 2009) has reported approximately 475 GRBs, i.e., a rate of about 250 per year. Over essentially the same period, only 17 bursts[3] have been identified by the *Fermi*/LAT. Given that roughly 50% of all GBM triggers point to directions within 66° of the LAT boresight, the fraction of bursts with photons above 100 MeV is apparently not much larger than 7%. Thus, it is an important task to apply the best possible techniques to explore whether this fraction would be significantly bigger if the detection threshold could be lowered. Such studies might significantly inform the design of future missions while extracting additional information from rather expensive facilities.

From launch through 2010 March 16, 55 GRBs have been detected (mainly by *Swift*, as well as *INTEGRAL*: Winkler et al. 2003; *AGILE*: Giuliani et al. 2008) at celestial coordinates that were simultaneously viewed by the *Fermi*/LAT. The angular resolutions of the *Swift* BAT and XRT are arcminutes and arcseconds, respectively. Compared with the mean point-spread width for the *Fermi*/LAT of a few degrees, these GRB coordinates are known with zero error. This sample is an excellent target for statistical methods that can take advantage of the precisely determined source direction. The basic technique that is employed here is the matched filter, most familiar to those detecting signals in the time domain. The underlying assumption of this method is that the characteristics of both the signal and background are a priori known functions of one or more variables. Since the matched filter maximizes the signal-to-noise ratio, moderate departures from optimality degrade the filter performance relatively slowly, making this a valuable tool for investigating the possible existence of faint signals. We present the sample and data processing in the following section, and details of the signal detection technique in Section 3. Results are given in Section 4 followed by a brief discussion in Section 5.

2. SAMPLE SELECTION AND DATA PROCESSING

A selection of 148 precisely located GRBs ($<1'.8$) was obtained from the *Swift* Web page[4] devoted to cataloging all

[3] http://fermi.gsfc.nasa.gov/ssc/observations/types/grbs/grb_table/

[4] http://swift.gsfc.nasa.gov/docs/swift/archive/grb_table.html/

bursts. The data correspond to the period from launch until the end of 2010 March. Most of these events were observed by the *Swift*/XRT, augmented by a few from *INTEGRAL* and *AGILE*. The resulting list was cross-correlated with *Fermi* spacecraft attitude data obtained from the *Fermi* Science Support Center[5] (FSSC) to identify only those events within 66° of the LAT boresight.

Having identified the principal focus of this investigation, two sets of LAT photon data were obtained from the FSSC corresponding to the 55 precisely located GRB fields and to 464 additional fields taken at random on the sky to study the background behavior. Throughout the following, they will be identified as "GRB" or "random" data. The FSSC data selection criteria corresponded to any of the three event classes, "transient," "source," or "diffuse," photon energies above 100 MeV but below 300 GeV, a zenith angle less than 105° and time intervals when the DATA_QUAL parameter was 1 and the South Atlantic Anomaly parameter, IN_SAA, was 0. The 105° zenith-angle limit might be considered a bit risky but with an orbiting altitude of 565 km, the Earth's limb appears at a zenith angle of 112.°83 which is easily resolvable. For the random LAT fields, fictitious GRB directions were chosen randomly over the sky but constrained by the less than 66° boresight requirement. Further cuts were imposed of less than 10.°5 for the angle between the photon and GRB directions and a time window spanning from $t_0 - 100$ s to $t_0 + 150$ s. With LAT point-spread width maxima of the order of 4°, the 10.°5 cut was imposed to allow up to 2.6σ errors without worrying about the effects of significant variations in the background flux over the effective solid angle of 0.105 sr. All data fields were additionally constrained to lie above or below the Galactic plane by more than 10°. Such additional criteria reduced the number of GRB fields from 55 to 41. Six of these have been previously associated with significant fluxes of energetic photons (>100 MeV) and thus provided guidance about the characteristics of the signals we were seeking.

3. SIGNAL DETECTION TECHNIQUE

The central theme of this paper is the use of a matched filter to enhance the signal-to-noise ratio for the detection of GRB photons in a diffuse background. There are four independent variables that are involved: energy (E), photon angle with respect to the GRB direction (θ), photon time of arrival (t), and photon event class ($c \in \{1, 2, 3\}$). The most obvious consideration is that the photon direction should be correlated with the GRB coordinates within an angle related to the LAT point-spread function (PSF) for that specific photon energy. Photons that fall far outside this criterion are almost certainly background. The energy criterion is less intuitive. The energy spectra for both the GRB signal and the background are approximately represented by decreasing power laws with exponents $\Gamma_{\rm GRB}$ and $\Gamma_{\rm back}$, respectively. Unfortunately, the background has a somewhat harder spectrum with $\Gamma_{\rm back} \simeq 1.5$ while $\Gamma_{\rm GRB} \simeq 2.2$. Thus, higher energy photons are more likely to represent background than signal. Photon directional accuracy is also critical, so photons with small uncertainty (i.e., high energy) should be weighted more heavily. The time filter is the most problematic because GRB light curves lack a uniform shape. Particularly for the most energetic burst photons, the time delay relative to the low-energy trigger can be substantial, up to thousands of seconds (Hurley et al. 1994). However, uniquely identifying such late quanta with a GRB can be problematic, especially in view of the lack of a distinguishing spectral characteristic. One feature that is generally observed is a prompt flux within a few seconds of the low-energy trigger. This can be seen in Figure 1 of Ghisellini et al. (2010). Most of the depicted LAT light curves exhibit a significant flux within 10 s of the burst. There are a few exceptions such as GRB 090328, so it must be recognized that not every fish can be caught with the same net. This led us to adopt a standard GRB light curve described by a broken power law with a break at $t_b = 5$ s. Prior to t_b, the flux rises as $(t/t_b)^{\alpha_0}$ after which it falls as $(t/t_b)^{-\alpha}$. The value for α_0 was set rather arbitrarily at 1/2, while α was picked to be 7/5 in concert with the general behavior of a large number of GRB afterglows. We emphasize that all the filter parameters were determined prior to applying them to either the GRB or random data sets.

When we began this analysis, we were unaware of the nuanced distinctions between the three LAT photon event classes, "transient," "source," and "diffuse," identified as 1, 2, and 3. Since we were looking for a transient point source, it seemed reasonable to include the "transient" quanta on equal footing with the other two. Only after going through the complete development of the matched filter search did we discover that the signal content of the "transient" photons is extremely small, ~3.5%. This was determined by looking at the event class photon counts for the most intense GRBs, 080916C, 090510, 090902B, and 091003. The ratio, $r_{\rm GRB}$, of "transient" and "source" GRB photons to "diffuse" is 0.34 and 0.44, respectively, roughly independent of the particular burst. On the other hand, the same ratios for the selected random LAT fields, $r_{\rm back}$, are 9.65 and 0.85. Consequently, we realized that we needed to include a weighting factor, w_c, based on event class that reflected this wide dispersion of information content. Serendipitously, the simple existence of a strong correlation of GRBs with "diffuse" class photons provided an independent verification of the validity of the matched filter technique.

From these considerations, the mathematical form of the matched filter weight functions is given by

$$w_E = \frac{1}{4\pi\sigma^2(E)} \left(\frac{E}{E_{\rm th}}\right)^{\Gamma_{\rm back}-\Gamma_{\rm GRB}} \tag{1}$$

$$w_\theta = 2e^{-\frac{\theta^2}{2\sigma^2(E)}} \tag{2}$$

$$w_t = \begin{cases} c \cdot \left(\dfrac{t}{t_b}\right)^{\alpha_0} & 0 \leqslant t \leqslant t_b \\ c \cdot \left(\dfrac{t}{t_b}\right)^{-\alpha} & t_b < t \leqslant t_c \\ c = 2.056382 \quad t_c = \frac{19}{2} t_b, \end{cases} \tag{3}$$

$$w_c = \left(\frac{r_{\rm GRB}(i)}{r_{\rm GRB}(3)}\right) \Big/ \left(\frac{r_{\rm back}(i)}{r_{\rm back}(3)}\right), \quad 1 \leqslant i \leqslant 3 \tag{4}$$

$$w(E, \theta, t, c) = w_E \cdot w_\theta \cdot w_t \cdot w_c. \tag{5}$$

The PSF for the LAT has been specified by the FSSC team in terms of a half-angle that includes 68% of a random sample. We have fit this to a power law in energy (Akerlof & Yuan 2007) to obtain separate parameter sets corresponding to conversion in either half of the LAT tracker using the form

$$\sigma_{68\%}(E) = \left(\frac{E}{E_{\rm th}}\right)^{-\delta} \sigma_0 + \sigma_1. \tag{6}$$

[5] http://fermi.gsfc.nasa.gov/ssc/

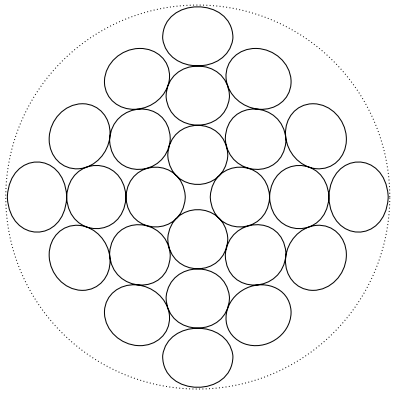

Figure 1. 10.°5 tiling of the LAT FoV. Twenty-four disks are closely confined within the 68° radius of the dotted circle that characterizes the acceptance of the LAT instrument.

For this analysis, we have assumed that the LAT PSF is Gaussian as described above for w_θ with a characteristic width determined by the containment condition:

$$\sigma_{\rm PSF}(E) = \frac{2}{3}\sigma_{68\%}(E). \quad (7)$$

Although the actual LAT angular error distribution function exhibits non-Gaussian tails, this approximation is unlikely to affect subsequent conclusions. As indicated above, the weight value for each photon is computed as a product of the four elements, w_E, w_θ, w_t, and w_c. The time filtering algorithm substantially ignores all photons that occur more than a few tens of seconds after the GRB trigger. For the parameters selected, this can best be described by an effective T_{90} window time for the signal of 16.864 s starting 1.624 s after the burst. The sum over all photons, $\sum w_i$, is the statistic used to identify events with significant fluxes of high-energy photons. In assessing this technique, the mean contribution from background photons turns out to be negligibly small. The identification problem is driven entirely by infrequent but large fluctuations of $\sum w_i$ contributed by background quanta. As an additional safeguard, a weight-sharing measure was introduced to ensure that the entire event weight was not generated by a single extreme photon. This parameter is defined by

$$\zeta = \frac{3(w_0 \cdot w_1 \cdot w_2)^{1/3}}{w_0 + w_1 + w_2}. \quad (8)$$

In this formula, w_0, w_1, and w_2 are the maximum three photon weights for a particular event. The combined statistic, $\zeta \sum w_i$, incorporates both the sum of photon weights and the additional requirement that no single photon contributes an overwhelming fraction of the value. The downside is that at least three photons must be associated with an event, an issue that will arise later.

The significances of the $\sum w_i$ and $\zeta \sum w_i$ statistics were determined by Monte Carlo simulations of the background. For each field of the GRB data set, 2000 events were generated using the measured background spectral distribution to determine energy and uniform distributions over solid angle and time to determine θ and t. The number of background photons for each field was set by the measured background rate. By looking at the weight statistics for simulated events with and without injected GRBs, we gained reasonable confidence that the matched filter algorithm would correctly identify a significant fraction of real bursts. This work also demonstrated that the modified sharing-compensated statistic, $\zeta \sum w_i$, was the stronger measure.

As described earlier, 41 GRB fields were selected for examination. These are listed in Table 2. Six of these events have been previously identified with >100 MeV LAT-detected photons. These are GRB 080916C (Abdo et al. 2009a), GRB 090323 (Ghisellini et al. 2010), GRB 090328A (Ghisellini et al. 2010), GRB 090510 (Abdo et al. 2009b), GRB 090902B (Abdo et al. 2009c), and GRB 091003 (Ghisellini et al. 2010).

The 35 GRB fields with no previous claims for LAT detections were the target of this investigation. We recognized that the most convincing argument for a true LAT identification should rely on the statistical distributions for the matched filter weights in LAT fields with similar characteristics. To increase that number as much as possible, the LAT fields of view (FoVs) were segmented into 24 circular tiles embedded on a spherical surface as shown in Figure 1. Each tile subtends a cone with a half-angle of 10.°5. This tiling scheme was applied to both the GRB and random field data sets to realize 697 and 8802 independent directions in space satisfying all the criteria described previously. Taking advantage of the fact that each field observation was blocked into a 250 s segment, the number of independent observations was multiplied by 5 by regarding each 50 s time slice as a separate sample. Thus, there are 3485 background measurements taken from LAT observations obtained simultaneously with the candidate GRB fields and an additional 44,010 samples taken under similar but not identical conditions. One particular concern for an analysis of this type is that false positives will selectively occur as the sample photon rate rises substantially above the mean. Evidence that this is not the case here is shown in Figure 2 which plots the cumulative distribution of the total number of photons within the LAT FoV over a 250 s interval. These rates explicitly exclude contamination from photons beyond the 105° zenith-angle cut. As shown in the plot, the two low-fluence GRB events reported here are not associated specifically with fields with high-ambient background rates. The similarity of the distributions for GRB and random fields also shows that the GRB data are not pathological as far as rates are concerned.

4. RESULTS

The statistical weighting scheme with the additional fractional sharing requirement clearly identified four of the six events previously associated with high-energy gamma-ray emission. The exceptions were GRB 090323 and GRB 0903028A for which photon counts were very sparse during the first 50 s following the burst trigger. Of the two, 090323 was marginally detected by the matched filter technique but GRB 0903028A provided no sign of a signal whatsoever. This gives some order of magnitude indication of the likely efficiency of the method. Three of the six were extremely intense with 100 or more energetic photons (GRB 080916C, GRB 090510, and GRB 090902B). As will be discussed later, the existence of such a substantial bright fraction is a rather surprising situation.

Most significantly, our analysis identified two additional bursts, GRB 080905A and GRB 091208B, as probably associated with energetic photon detections in the LAT. The best estimate for the probability of these occurring by chance alone was obtained by performing identical searches on random LAT fields with the same criteria. Thus, 1 out of 44,010 random fields generated matched filter weights exceeding the value for GRB 080905A and 11 similar fields generated weights exceeding the value for GRB 091208B. Multiplying by a trial factor

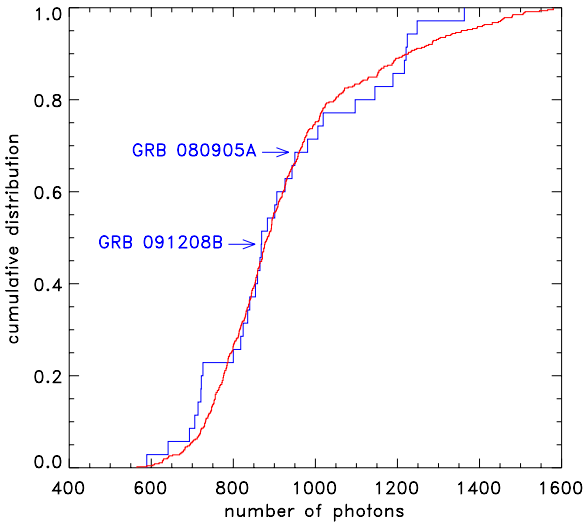

Figure 2. Cumulative distributions of LAT photon rates over 250 s intervals for the GRB (blue) and random background (red) fields. These rates reflect the entire LAT FoV except for photons that lie outside the 105° zenith-angle cut. The rates corresponding to the two claimed GRB detections are indicated by arrows.

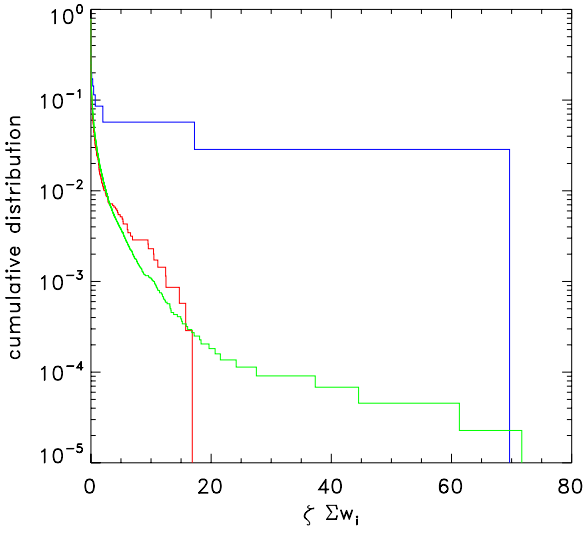

Figure 3. Complements of the cumulative distributions for $\zeta \sum w_i$ for 35 well-localized GRB fields (blue), 3485 random fields obtained nearly simultaneously with the GRB data (red), and 44,010 random fields obtained at random times (green).

of 35 for the number of localized fields considered, the associated probabilities are 8.0×10^{-4} and 8.7×10^{-3}. To check that these correlations were simply not due to preferentially higher background rates for the GRB exposures, we also performed similar calculations for the LAT data confined to ∼20 uncorrelated directions and five independent time intervals from the same GRB data sets. All of these results are plotted as cumulative distributions in Figure 3. The statistical similarity of the GRB off-axis and random field data demonstrates that the GRB data set is not correlated with anomalous environmental conditions such as higher cosmic ray background rates. A list of photons associated with these two events is provided in Table 1.

Two independent observations at significance levels of 0.1% and 1% already make this a reasonably credible result. However, as we discovered the importance of LAT "diffuse" photons for identifying point sources such as GRBs, we realized that independent of the matched filter weight analysis, a simple count

Table 1
List of High-energy Photons for GRB 080905A and GRB 091208B

i	t (s)	θ (°)	E (MeV)	c	w_i
GRB 080905A		$\zeta = 0.2118$			$\zeta \sum w_i = 69.66$
1	10.019	0.21	474	3	267.07
2	5.661	2.27	181	3	61.06
3	6.727	10.41	103	2	0.77
GRB 091208B		$\zeta = 0.8442$			$\zeta \sum w_i = 17.23$
1	17.932	2.06	131	3	11.18
2	20.985	2.72	125	2	3.94
3	4.968	1.66	544	1	3.02
4	6.364	1.16	1179	1	2.07
5	19.735	7.17	197	3	0.20

of the number of such quanta was statistically quite significant. Thus, for the 35 well-localized GRB fields that do not include the previously reported LAT-detected GRBs, the total number of "diffuse" photons is 25 for a rate of 0.714 ± 0.143. For the GRB off-axis fields and the random fields, the comparable numbers are 1384 for 3485 fields and 17,414 for 44,010 to yield per field rates of 0.397 ± 0.011 and 0.396 ± 0.003. The random probability of such differences is less than 2.7%. As can be seen from the lists of photon counts in Tables 1 and 2, the two new GRB identifications are strongly correlated with these "diffuse" photons as well. Thus, the combined probability that these claims might be randomly generated must be less than 1×10^{-5}.

GRB 080905A is a short burst with optical counterparts and a redshift of 0.128 (Rowlinson et al. 2010), while GRB 091208B is a long burst also with optical counterparts (Pagani et al. 2010) and a redshift of 1.063 (Wiersema et al. 2010; Perley et al. 2010). As listed in Table 1, the estimated number of >100 MeV photons for each event is about 3. This is substantially lower than any previous LAT GRB identifications. Estimating the corresponding fluence of >100 MeV photons raised some interesting statistical issues that are perhaps not well appreciated. To first order, one would anticipate simply adding up all the energies of the detected quanta and dividing by the effective detector area. Although this produces a number, it bears only a casual relation to the intrinsic properties of the GRB in question. The reason is that the spectral number distribution, dN/dE follows a power law with exponent between −3 and −2. Thus, the mathematical mean is defined but the variance is infinite. This leads to the conclusion that sums of energies drawn from the identical parent population will vary by factors of the order of unity, independent of the number of photons in the sample. In our case, the statistical uncertainty is already substantial since only three photons are detected for each event. Thus, we opted for a solution that invoked the least number of new assumptions: we adopted the LAT fluence values for bright bursts computed by Ghisellini et al. (2010) and listed in their Table 1. We next assumed that the spectral distribution for all bursts was an approximately universal function of energy so that fluences would scale with photon number. This led to estimates of the LAT fluence value of 3×10^{-6} erg cm^{-2} for both events. Unfortunately, the proportionality of fluence to photon counts is not very evident. As can be seen in Table 2 for the two bursts, GRB 090510 and GRB 090902B, for essentially the same number of photons, the fluences differ by a factor of 16. This problem may require a better realization of how fluences should be estimated. For future purposes when dealing with events with more numerous quanta, there is a robust measure of

Table 2
List of 41 Precisely Located LAT-observed GRBs

i	GRB	T_{90} (s)	UT	Trigger[a]	α[b] (°)	δ[c] (°)	$\theta_{\rm zenith}$[d] (°)	$\theta_{\rm bore}$[e] (°)	b[f] (°)	$n_{\rm total}$[g]	n_1[h]	n_2[h]	n_3[h]	$\zeta\sum w_i$[i]	$S_{\rm GBM}$[j] (μerg cm^{-2})	$S_{\rm LAT}$[k] (μerg cm^{-2})
Previously reported GRBs with LAT-detected photons																
1	080916C	100.9	00:12:45	*Fermi*/GBM	119.847	−56.638	83.657	48.838	−13.760	916	26	31	85	7910.540	120.00	70
2	090323	70.0	00:02:42	*Fermi*/GBM	190.709	17.054	69.558	59.538	79.731	763	2	0	2	10.570	100.00	36
3	090328A	100.0	09:36:46	*Fermi*/GBM	90.665	−41.883	71.005	64.538	−26.384	932	4	2	1	0.606	80.90	33
4	090510	0.3	00:23:00	351588	333.553	−26.583	52.541	13.468	−55.074	898	26	48	112	31389.817	21.00	37
5	090902B	21.0	11:05:08	*Fermi*/GBM	264.939	27.325	41.225	50.954	26.911	1088	54	49	93	8530.459	352.00	590
6	091003	21.1	04:35:45	*Fermi*/GBM	251.520	36.625	62.298	12.306	40.055	1062	8	2	7	1107.330	37.60	13
New candidate GRBs with LAT-detected photons																
7	080905A	1.0	11:58:54	323870	287.674	−18.880	30.418	29.860	−12.605	950	2	1	3	69.660	0.56	3
8	091208B	14.9	09:49:57	378559	29.392	16.890	28.815	55.885	−43.150	868	2	1	3	17.227	5.80	3
GRBs with no significant LAT-detected photons																
9	080804	34	23:20:14	319016	328.668	−53.185	83.852	58.149	−48.369	641	0	0	0	0	*6.00	
10	080810	106	13:10:12	319584	356.794	−0.320	29.913	62.123	−59.066	1019	1	0	0	0	6.90	
11	080906	147	13:33:16	323984	228.042	−80.518	71.429	36.599	−19.264	1189	11	1	1	0.034	*5.83	
12	080916B	32	14:44:47	324907	163.665	69.065	55.357	27.941	44.707	1248	9	0	1	1.975	10.90	
13	080928	280	15:01:32	326115	95.070	−55.200	76.016	45.239	−26.313	726	3	0	1	0	3.50	
14	081003A	∼30	13:46:12	*INTEGRAL*	262.391	16.571	21.858	56.387	25.363	926	2	0	1	0	...	
15	081012	29	13:10:23	331475	30.201	−17.638	68.915	61.566	−71.399	721	1	0	0	0	4.30	
16	081016B	2.6	19:47:14	331856	14.564	−43.530	83.851	65.064	−73.540	1224	2	0	0	0	*0.17	
17	081029	270	01:43:56	332931	346.773	−68.156	79.789	57.063	−46.109	981	3	0	1	0.001	*3.50	
18	081104	59.1	09:34:42	333666	100.489	−54.720	66.142	32.627	−23.173	835	3	0	1	0	*3.33	
19	081118	67	14:56:36	334877	82.593	−43.301	65.099	30.522	−32.485	706	2	1	0	0.001	0.11	
20	081127	37	07:05:08	335715	332.064	6.851	20.654	52.608	−37.920	869	2	0	0	0	*0.82	
21	081222	24	04:53:59	337914	22.741	−34.096	29.145	51.259	−79.017	714	7	1	2	0.447	13.50	
22	090113	9.1	18:40:39	339852	32.057	33.429	21.263	32.518	−26.760	883	3	0	2	0	*1.27	
23	090407	310	10:28:25	348650	68.979	−12.679	13.189	34.739	−35.741	800	3	1	0	0	*1.83	
24	090516A	210	08:27:50	352190	138.261	−11.854	11.567	31.509	24.261	1217	6	0	0	0	23.00	
25	090518	6.9	01:54:44	352420	119.954	−0.759	33.312	49.588	14.806	854	2	0	1	0	1.60	
26	090519	64	21:08:56	352648	142.279	−0.180	51.625	50.424	34.312	693	3	1	0	0.018	*2.00	
27	090529	>100	14:12:35	353540	212.469	24.459	80.559	23.511	72.163	589	11	0	0	0.017	*1.13	
28	090702	∼10	10:40:37	*INTEGRAL*	175.897	11.502	80.386	62.327	67.683	859	1	0	0	0	...	

Table 2
(Continued)

i	GRB	T_{90} (s)	UT	Trigger[a]	α[b] (°)	δ[c] (°)	$\theta_{\rm zenith}$[d] (°)	$\theta_{\rm bore}$[e] (°)	b[f] (°)	$n_{\rm total}$[g]	n_1[h]	n_2[h]	n_3[h]	$\zeta\sum w_i$[i]	$S_{\rm GBM}$[j] (μerg cm^{-2})	$S_{\rm LAT}$[k] (μerg cm^{-2})
29	090708	15.0	03:38:15	356776	154.632	26.616	79.492	56.487	56.031	1006	1	0	0	0	0.40	
30	090709B	27.2	15:07:42	356912	93.522	64.081	85.836	46.897	20.304	818	2	1	1	0.025	1.30	
31	090712	145	03:51:05	357072	70.097	22.525	60.746	33.281	−15.676	865	8	1	0	0.715	4.20	
32	090728	59	14:45:45	358574	29.653	41.633	90.838	60.660	−19.505	1221	2	0	0	0	*1.67	
33	090813	7.1	04:10:43	359884	225.779	88.568	72.707	35.418	28.328	824	2	0	0	0	3.50	
34	091010	8.1	02:43:09	*AGILE*	298.666	−22.518	68.465	55.714	−23.488	1145	3	0	3	0.001	10.90	
35	091127	7.1	23:25:45	377179	36.583	−18.953	54.011	25.423	−66.738	840	8	0	1	0.130	18.70	
36	091202	∼50	23:10:12	*INTEGRAL*	138.834	62.550	69.166	23.256	40.214	906	7	0	1	0.289	...	
37	091221	68.5	20:52:52	380311	55.797	23.241	87.598	53.620	−24.755	943	4	0	0	0	13.80	
38	100111A	12.9	04:12:49	382399	247.048	15.551	48.142	33.854	38.604	1363	6	0	2	0	1.50	
39	100206A	0.12	13:30:05	411412	47.162	13.157	49.423	44.608	−37.742	1097	6	0	0	0.001	0.93	
40	100212A	136	14:07:22	412081	356.418	49.494	56.829	23.422	−11.989	901	4	0	0	0	0.38	
41	100316D	∼740	12:44:50	416135	107.628	−56.255	90.330	50.079	−19.759	722	5	0	0	0	*0.50	

Notes.

[a] *Swift* trigger number if numeric; otherwise satellite name.

[b] GRB right ascension.

[c] GRB declination.

[d] Angle between the local orbit zenith direction and GRB.

[e] Boresight angle of GRB with respect to the LAT principal axis.

[f] GRB Galactic latitude.

[g] Total number of LAT-detected photons over 250 s interval excluding those beyond 105° zenith-angle cut.

[h] n_1, n_2, and n_3 are the number of photons within 10.°5 of the GRB direction in 47.5 s window.

[i] Total event matched filter weight including the sharing parameter, ζ.

[j] GBM fluence, $S_{\rm GBM}$, calculated as described in the main text. * indicates an entry with no available GBM fluence measurement; the value is estimated from the BAT fluence by multiplying by a factor of 1.67, as derived from a joint sample of BAT and GBM measurements. Most other fluence values were taken from Table 2 in Guetta et al. (2010). The exceptions were obtained from the following references: GRB 080905A, Bissaldi et al. (2008); GRB 081118, Bhat et al. (2008); GRB 090510, Guiriec et al. (2009); GRB 090518, Paciesas (2009); GRB 100206A, von Kienlin (2010).

[k] LAT fluence, $S_{\rm LAT}$, calculated as described in the main text.

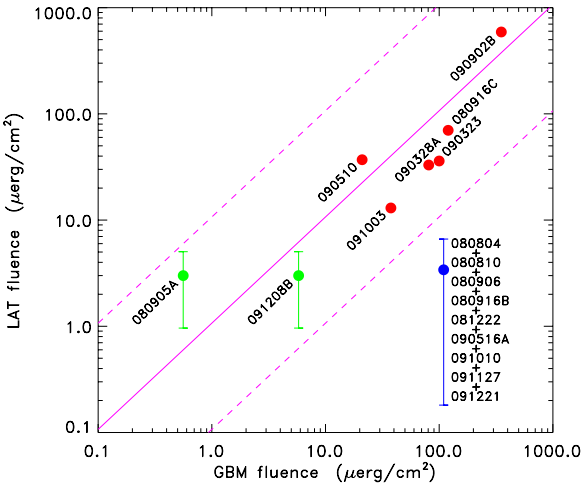

Figure 4. Plot of high-energy (LAT) fluences vs. low-energy (GBM) fluences for the bursts considered in this paper. The six red points indicate the events previously reported by the LAT team. The two green points were identified by the matched filter technique. The solid magenta line is a linear fit to the six LAT-detected bursts, 080916C, 090323, 090328A, 090510, 090902B, and 091003. The dashed lines above and below indicate LAT fluences 10 times greater and smaller. The blue point is the co-added sum of nine GRBs with GBM fluences comparable to or greater than GRB 091208B, i.e., greater than 5 μerg cm^{-2}. The abscissa is the sum of all nine GBM fluences and the ordinate is estimated from the total of all event class 2 and 3 photons in the corresponding burst fields. This indicates a significant population with high-energy fluences below the approximately 1:1 fluence ratio represented by the diagonal solid magenta line.

fluence: multiply the number of photons by the median energy. In the continuum limit, a power-law distribution generates the following relation between $E_{\rm mean}$ and $E_{\rm median}$ over the interval from threshold to infinity:

$$E_{\rm mean} = \frac{\Gamma - 1}{\Gamma - 2}\frac{1}{2^{\Gamma-1}} E_{\rm median}. \quad (9)$$

Thus, a robust proxy for gamma-ray burst fluence can be obtained by multiplying this estimate of $E_{\rm mean}$ by the number of detected photons.

The fact that >100 MeV photons have been observed with both long and short bursts suggests that the production mechanism is generic to relativistic jets, independent of the detailed structure of the progenitor system. So far, most of the high-energy photon observations have been associated with large fluences at the lower energies measured by the *Swift*/BAT and the *Fermi*/GBM detectors. To explore such fluence correlations, Figure 4 shows a scatterplot of LAT fluences versus GBM fluences for the six bright bursts previously identified by the LAT collaboration, the two bursts uncovered by the statistical analysis described in this paper and the co-added sum of nine bursts with no strong perceptible radiation above 100 MeV. For these purposes, GBM fluences were defined by photons in the range of 8–1000 keV within the T_{90} time interval. The LAT fluences were obtained from Ghisellini et al. (2010) and the scaling method described previously.

The salient feature of Figure 4 is the overall linear correlation of the LAT and GBM fluences with a ratio of unity between the two. The short burst identified by our analysis, GRB 080905A, lies above the trend line, a feature previously noted for this class of events (see the discussion of GRB 081024B in Abdo et al. 2010 and GRB 090510 in Ackermann et al. 2010). GRB 091208B is completely consistent with the higher fluence events. An interesting aspect of this graph is the estimate for the total co-added LAT fluence for nine bursts with GBM fluences roughly equal to or greater than GRB 091208B, but which lie a factor of 10 lower but with rather large errors. If one believes that all GRBs have a similar generic behavior, it is possible that a large fraction of these events have delayed high-energy emission that evades our estimates. It is more likely that there is a real population difference between events such as 080916C, 090926A, and 091208B and the majority of all other GRBs. Examining this question with larger data sets may shed some light on the mechanisms that drive high-energy emission processes.

Although the statistics are admittedly crude, we can use this analysis to set some limits on the fraction of high-energy photon GRBs at the present levels of sensitivity. Starting with a sample of 41 well-localized events, we have identified two with high statistical significance. The remaining number of LAT "source" and "diffuse" photons above background is no more than approximately three. The efficiency of this technique is about 50% for a total, so as many as 16 GRBs out of 41 fields could be associated with >100 MeV photons. Thus, instead of 17 LAT-detected GRBs over a two-year period, there might be 45 events or 19% of all viewable GBM triggers with a lower limit of 25 events or 11% of the total. That is lower than any estimates prior to the *Fermi* launch.

5. DISCUSSION

By using optimal signal detection techniques, we have demonstrated that the existence of GRB high-energy photon emission can be extended downward in brightness by a significant factor. Increasing the dynamic range over which such phenomena can be measured puts a number of constraints on physical models that can describe these events. As we have shown, these statistical methods can set interesting limits on the behavior of ensembles of events at lower levels than is possible for single isolated bursts, raising serious questions about the homogeneity of the GRB phenomenon. After another two years in orbit, the *Fermi* data will increase enough to allow more careful re-examination of the initial conclusions presented here.

The most surprising aspect of this work is the very small number of GRBs that could be positively identified with high-energy emission as a result of the substantially lower fluence thresholds. Almost any model would anticipate an increase in number proportional to the inverse of the ratio of detection thresholds raised to the power of unity or greater. Monte Carlo estimates indicate that our detection efficiency was of the order of 50% for the two events reported. This does not come close to explaining the apparent deficit of low-intensity events compared to the number of bursts similar to GRBs 080916C, 090510, and 090902B. We look forward to pursuing this problem during this precious and unique period when both *Fermi* and *Swift* are working magnificently.

We thank Chris Shrader, director of the *Fermi* Science Support Center for his considerable help in obtaining and interpreting the *Fermi* mission data products. Fang Yuan provided valuable assistance in the initial process of learning how to access and manipulate the *Fermi* data. This research is supported by NASA grant NNX08AV63G and NSF grant PHY-0801007.

REFERENCES

Abdo, A. A., et al. 2009a, Science, 323, 1688
Abdo, A. A., et al. 2009b, Nature, 462, 331

Abdo, A. A., et al. 2009c, ApJ, 706, L138
Abdo, A. A., et al. 2010, ApJ, 712, 558
Ackermann, M., et al. 2010, ApJ, 716, 1178
Akerlof, C. W., & Yuan, F. 2007, arXiv:astro-ph/0702295v2
Atwood, W. B., et al. 2009, ApJ, 697, 1071
Band, D., et al. 2009, ApJ, 701, 1673
Bhat, P. N., et al. 2008, GCN Circ., 8550
Bissaldi, E., et al. 2008, GCN Circ., 8204
Catelli, J. R., Dingus, B. L., & Schneid, E. J. 1998, in AIP Conf. Proc. 428, Fourth Huntsville Gamma-ray Burst Symposium, ed. C. A. Meegan (Melville, NY: AIP), 309
Dingus, B. L. 2003, in AIP Conf. Proc. 662, Gamma-ray Burst and Afterglow Astronomy 2001: A Workshop Celebrating the First Year of the HETE Mission, ed. G. R. Ricker & R. K. Vanderspek (Melville, NY: AIP), 240
Gehrels, N., et al. 2004, ApJ, 611, 1005
Ghisellini, G., et al. 2010, MNRAS, 403, 926
Giuliani, A., et al. 2008, A&A, 491, L25
Guetta, D., et al. 2011, A&A, 525, A53
Guiriec, S., et al. 2009, GCN Circ., 9336
Hurley, K., et al. 1994, Nature, 372, 652
Meegan, C., et al. 2009, ApJ, 702, 791
Paciesas, W. 2009, GCN Circ., 9419
Pagani, C., et al. 2010, GCN Circ., 10256
Perley, D. A., et al. 2010, GCN Circ., 10272
Rowlinson, A., et al. 2010, MNRAS, 408, 383
von Kienlin, A. 2010, GCN Circ., 10381
Wiersema, K., et al. 2010, GCN Circ., 10263
Winkler, C., et al. 2003, A&A, 411, L1